Presence of mutant p53 increases stem cell frequency and is associated with reduced binding to classic TP53 binding sites in cell lines and primary AMLs

Gerritsen, Mylène; Hilgendorf, Susan; Yi, Guoqiang; Wierenga, Albertus T J; Schuringa, Jan-Jacob; Martens, Joost H A; Vellenga, Edo

Published in:
Experimental Hematology

DOI:
10.1016/j.exphem.2022.03.007

Publication date:
2022

Presence of mutant p53 increases stem cell frequency and is associated with reduced binding to classic TP53 binding sites in cell lines and primary AMLs

Mylène Gerritsen[a,1]*, Susan Hilgendorf[a,1], Guoqiang Yi[b], Albertus T.J. Wierenga[a], Jan-Jacob Schuringa[a], Joost H.A. Martens[b], and Edo Vellenga[a]

[a]*Department of Hematology, University Medical Centre Groningen, University of Groningen Cancer Research Centre, Groningen, The Netherlands;* [b]*Department of Molecular Biology, Radboud Institute for Molecular Life Sciences (RIMLS), Radboud University, Nijmegen, The Netherlands*

With an overall 5%–10% incidence rate in acute myeloid leukemia (AML), the occurrence of *TP53* mutations is low compared with that in solid tumors. However, when focusing on high-risk groups including secondary AML (sAML) and therapy-related AMLs, the frequency of mutations reaches up to 35%. Mutations may include loss of heterozygosity (LOH) or deletion of the 17p allele, but are mostly missense substitutions that are located in the DNA-binding domain. Despite elaborate research on the effects of *TP53* mutations in solid tumors, in hematological malignancies, the effects of *TP53* mutations versus loss of *TP53* remain unclear and under debate. Here, we compared the cellular effects of a *TP53* mutant and loss of *TP53* in human hematopoietic stem and progenitor cells (HSPCs). We found that when expressing *TP53* mutant or loss of *TP53* using siRNA, $CD34^+/CD38^-$ cells have a significantly enhanced replating potential, which could not be demonstrated for the $CD34^+/CD38^+$ population. Using RNA-sequencing analysis, we found a loss of expression of p53 target genes in cells with *TP53* knockdown. In contrast, an increased expression of a large number of genes was observed when expressing *TP53* mutant, resulting in an increase in expression of genes involved in megakaryocytic differentiation, plasma membrane binding, and extracellular structure organization. When binding of p53 wild type and p53 mutant was compared in cell lines, we found that mutant p53 binds to a large number of binding sites genomewide, contrary to wild-type p53, for which binding is restricted to genes with a p53 binding motif. These findings were verified in primary AMLs with and without mutated *TP53*. In conclusion, in our models, we identified overlapping effects of *TP53* mutant and loss of *TP53* on in vitro stem cell properties but distinct effects on DNA binding and gene expression.

HIGHLIGHTS

- *TP53* mutant or loss of *TP53* results in enhanced replating potential in HSCs.
- Mutant p53 proteins have altered DNA binding patterns in primary AML.
- P53 mutant leads to increased expression of a number of target genes, suggesting "gain-of-function" effects.

INTRODUCTION

Disruption of p53 function can be caused by loss of the short arm of chromosome 17 where *TP53* is located or by the presence of *TP53* mutations [1]. Most mutations are missense substitutions and are located in the DNA-binding domain, which is home to the six most commonly found "hotspot" mutations [2,3]. Several hotspot mutations are more commonly found than others, suggesting that not all mutant forms of p53 exert the same effects. These mutations lead to loss of tumor-suppressive functions of wild-type p53, but *TP53* mutations have also been associated with oncogenic gain-of-function (GOF), which is known to alter gene expression and is probably related to altered protein stability [3–5]. Several genes that have been previously described as being regulated by mutant p53—but not by wild-type p53—include *MYC* and *FOS* [3]. In addition, it has been determined that GOF p53 binds to the promoters of chromatin modifiers *KMT2A* (MLL1), *KMT2D* (MLL2), and *KAT6A* (MOZ) and induces their expression [6]. Recently, Chen et al. [7] described that *TP53* mutations drive clonal hematopoiesis in

Offprint requests to: Mylène Gerritsen. Present adress: Laboratory of Hematology (Huispost 475), Department of Laboratory Medicine, Radboud University Medical Center, Geert Grooteplein zuid 8, 6525 GA Nijmegen, The Netherlands; E-mail: mylene.gerritsen@radboudumc.nl.

(Received 21 June 2021; revised 6 March 2022; accepted 9 March 2022)

[1]MG and SH contributed equally to this work.

https://doi.org/10.1016/j.exphem.2022.03.007

response to cellular stressors in murine models. They found that mutant p53 interacts with EZH2, which in turn enhances its association with the chromatin, increasing the levels of H3K27me3 in genes regulating HSC self-renewal and differentiation, suggesting also a GOF effect. On the contrary, Boettcher et al. [8] suggested that the effects of p53 are due mainly to a dominant negative activity by constructing isogenic acute myeloid leukemia (AML) cell lines carrying different *TP53* mutations.

In contrast to solid tumors, *TP53* mutations are relatively rare in AML and affect only 5% to 10% of de novo AML, but are more frequently observed in high-risk groups [9–11]. In line with other cancers, in hematological malignancies *TP53* mutations are often heterozygous point mutations, but loss of heterozygosity (LOH) or deletion of the second allele (17p) also is a frequent event [12]. Recent research in murine models has indicated that the combination of a *TP53* mutation with a 17p deletion results in an even more unfavorable prognosis than the *TP53* mutation alone [13]. Together, these findings suggest that, at least in hematological malignancies, the effects of *TP53* mutations versus loss of *TP53* remain unclear and under debate. In the present study, we investigated the cellular effects of *TP53* mutant R273H, a mutational hotspot mutant, and loss of *TP53* in human hematopoietic stem and progenitor cells (HSPCs) in conjunction with RNA sequencing to elucidate the differences in gene expression. These findings were verified in AML cell lines and patient AML samples by using chromatin immunoprecipitation (ChIP) sequencing to identify differential binding of p53 mutant in primary *TP53* mutant AMLs.

METHODS

Primary cells and cell lines

Umbilical cord blood (CB) was derived from healthy full-term pregnancies from the obstetrics departments of the Martini Hospital and University Medical Center in Groningen, The Netherlands, after patients provided informed consent. $CD34^+$ cells were isolated by MACS separation (Miltenyi, Leiden, Netherlands). $CD34^+$ cells were maintained in Stemline II (Sigma-Aldrich, Amsterdam, Netherlands), supplemented with 100 ng/mL stem cell factor (SCF, c-kit ligand), 100 ng/mL thyropoietin (TPO), and 100 ng/mL Fms-like tyrosine kinase receptor 3 (FLT3) ligand until further use (24–48 hours). AML cells from peripheral blood or bone marrow from AML patients was studied after informed consent was obtained in accordance with the Declaration of Helsinki. The protocol was approved by the Ethical Review Board of the University Medical Center Groningen, Groningen, The Netherlands. The mononuclear cell (MNC) fraction was obtained by density gradient centrifugation using lymphoprep (PAA, Cölbe, Germany) according to standard procedures. Two *TP53* mutant AMLs were selected to have a variant allele frequency (VAF) of approximately ≥50% in bone marrow.

MOLM13, NB4, and OCI-AML3 were cultured in RPMI-1640 (Gibco, The Netherlands) supplemented with 10% fetal calf serum (FCS) and 1% penicillin/streptomycin. Mono-Mac-6 cells were cultured in RPMI-1640 supplemented with 10% FCS, 1% penicillin/streptomycin (Gibco//Life Technologies Europe BV, Bleiswijk, Netherlands), nonessential amino acids (NEAA, Sigma-Aldrich), and 10 μg/mL human insulin (Sigma-Aldrich).

Plasmid construction and lentiviral transduction

TP53 constructs were created by polymerase chain reaction (PCR) from cDNA from *TP53* mutant and wild-type cell lines (MDA-MB-468 harbors $TP53^{R273H}$; MOLM13 was used for wild-type *TP53*) and subcloned into a pRRL–SFFV–iGFP vector, and the correct insert was validated by sequencing. Lentiviral particle production was performed using Fugene (Promega Benelux, Leiden, Netherlands), and transduction of CB cells was performed using 2 μg/mL polybrene (Sigma-Aldrich). After 48–72 hours, cells were sorted on GFP^+ and/or $CD34^+CD38^-$ cell fractions (CD34-BV421, CD38-PE, BD Biosciences, Vianen, Netherlands) on MoFlo XDP or Astrios (Dako Cytomation, Carpinteria, CA).

CFC assays, liquid cultures, MS5 stromal cocultures, and LTC-IC

Colony-forming cell formation analysis was performed by plating 1,000 $CD34^+$ cells in methylcellulose (H4230, StemCell Technologies, Saint-Egreve, France), supplemented with 20 ng/mL interleukin-3 (IL-3), 20 ng/mL IL-6, 20 ng/mL colony-stimulating factor granulocyte (G-CSF), 20 ng/mL stem cell factor (SCF), and 6 U/mL erythropoietin (EPO). CFU-G, CFU macrophage (CFU-M), and burst forming units erythroid (BFU-E) colonies were scored after 10–14 days of culture. Long-term culture-initiating cell assay (LTC-IC) was performed by sorting transduced cord blood (CB $CD34^+$) cells in limiting dilutions in the range 6–1,458 cells per well on MS5 stromal cells in a 96-well plate in Gartners LTC medium (α-modified Minimum Essential Medium [αMEM], Lonza, Basel, Switzerland) supplemented with 12.5% heat-inactivated FCS, heat-inactivated 12.5% horse serum (Sigma-Aldrich), penicillin and streptomycin (Gibco, The Netherlands), 57.2 μmol/L β–mercaptoethanol (Sigma-Aldrich), and 1 μmol/L hydrocortisone (Sigma-Aldrich), and half of the medium was replenished weekly. After 5 weeks, methylcellulose was added to the wells. One to 1.5 weeks later, wells containing colonies were scored as positive.

Protein stability assay and immunoblotting

Protein stability was determined by treating cells for different time points with 0.1mg/mL cycloheximide (Sigma-Aldrich, No. C7698). Whole-cell extracts were prepared by boiling an appropriate amount of cells in Laemmli sample buffer for 5 min with subsequent separation on 10% sodium dodecyl sulfate (SDS)–acrylamide gels. Proteins were transferred to polyvinyl difluoride (Millipore, Netherlands) using wet transfer. p53 was detected with α-P53 DO-1 sc-126X antibody (Santa Cruz, Germany).

RNA extraction and Illumina high-throughput sequencing

RNA was isolated by separation of the aqueous phase with TRIzol Reagent (ThermoFisher, Bleiswijk, Netherlands) according to the manufacturer's protocol. The aqueous phase was mixed with 70% ethanol (1:1), and isolation was continued using the RNeasy microkit (Qiagen, Hilden, Germany) including on-column DNase I treatment. RNA libraries were prepared using the KAPA RNA HyperPrep Kit with RiboErase (HMR) according to the manufacturer's protocol (KR1351–v1.16, Roche Sequencing Solutions). In brief, 25 ng to 1 μg of input RNA was depleted from ribosomal RNA by oligohybridization, RNaseH treatment, and DNase digestion. rRNA-depleted RNA was fragmented to ~200-bp fragments, and first-strand

synthesis was performed using random primers. The second strand was synthesized using dUTP for strand specificity. After adapter ligation, library amplification was performed, and the number of cycles was dependent on the amount of starting material. A bioanalyzer using a high-sensitivity DNA Chip (Agilent) was used to check fragment size. Samples were sequenced on an Illumina NextSeq 500 system with 2×43-bp paired-end sequencing (PE43).

Data retrieval

Differential gene expression of *TP53*mut AMLs was determined from in-house samples (Blueprint, Supplementary Table E1, online only, available at www.exphem.org) [14,15]. ($n = 39$, $TP53^{mut} = 6$); the TCGA data set [11,16] ($n = 179$, $TP53^{mut} = 20$); and the BeatAML data set [17] ($n = 494$, $TP53^{mut} = 26$) [17].

Chromatin immunoprecipitation and sequencing

Primary AML cells and cell lines were crosslinked with 1% formaldehyde for 10 min at room temperature at a concentration of 30×10^6 cells/mL. The fixed cells were sonicated 10−15 cycles (30 sec on, 30 sec off) to a size of 200−600 bp. Sonicated chromatin was incubated overnight with either 5 μg TP53 antibody (Santa Cruz: DO-1, sc-126X) or 2 μg of antibody against H3K4me3, H3K27me3, or H3K27ac. The next day, antibody−protein complexes were bound to magnetic Protein G beads (Invitrogen, ThermoFisher, Netherlands) for ~2 hours. Beads were washed with four different wash buffers, and chromatin was eluted from the beads. DNA proteins were decrosslinked, and samples were purified using the Qiaquick MinElute PCR purification kit. Sequencing samples were prepared according to the manufacturer's protocol (Illumina, Eindhoven, Netherlands). End repair was performed using the precipitated DNA using Klenow and T4 PNK, and subsequently a 3′ protruding A base was generated using Taq polymerase followed by adapter ligation. The DNA was amplified by PCR and ~300 bp (ChIP fragment + adapters). Samples were sequenced on an Illumina NextSeq 500 system with 2×43 bp paired-end sequencing (PE43).

Statistical analysis

A paired or unpaired two-sided Student *t* test was used to calculate statistical differences. A p value < 0.05 was considered to indicate statistical significance. Error bars represent standard deviations: $^*p < 0.05$, $^{**}p < 0.01$, $^{***}p < 0.001$.

RESULTS

To understand how mutant p53 affects human hematopoietic cells and contributes to malignant transformation we created an overexpression construct expressing the missense mutant R273H ($p53^{R273H}$), one of the six most common *TP53* mutations in human cancers (Supplementary Figure E1A, online only, available at www.exphem.org). We confirmed the enhanced stability of $p53^{R273H}$ in the cell line OCI-AML3 by expressing $TP53^{wt}$ or $TP53^{R273H}$ followed by cycloheximide treatment, whereas $p53^{wt}$ was completely degraded after 60 min of treatment, $p53^{R273H}$ remained stable within this time frame (Supplementary Figure E1B, online only).

To understand the cellular programs induced by $p53^{R273H}$, $CD34^+$ umbilical CB cells were transduced with either a $TP53^{R273H}$ overexpression vector or control vector (control) (Figure 1A). In vitro colony assays revealed that $TP53^{R273H}$ overexpression in CB $CD34^+$ cells provided a more than twofold loss of erythroid colony formation, while the myeloid lineage exhibited a significantly enhanced replating potential of granulocyte and macrophage colony formation (CFU-G/M) (Figure 1B). To define the cell population that contributes to this replating potential, we sorted $CD34^+/CD38^-$ and $CD34^+/CD38^+$ and repeated this experiment. We found that the $CD34^+/CD38^-$ sorted $TP53^{R273H}$ cells did have a significantly enhanced replating potential that could not be demonstrated in $TP53^{R273H}$ sorted $CD34^+/CD38^+$ cells or control cells (Figure 1C). This suggests that the stem cell−enriched fraction ($CD34^+/CD38^-$) is particularly susceptible to the effects of mutant p53. These findings are in line with the results of a long-term culture initiating colony (LTC-IC) assay, which revealed a significantly enhanced stem cell frequency (Figure 1D).

As the unfavorable prognosis of *TP53*-mutated AML is associated not only with mutations, but also with loss of heterozygosity (LOH) or deletion of the second allele (17p), we investigated whether loss of *TP53* yielded comparable phenotypes in HSPCs. CB $CD34^+$ cells were transduced with RNAi against *TP53* (sh*TP53*) or control (shSCR), which causes a 95% reduction in *TP53* expression (Figure 2A). Similar to the $TP53^{R273H}$, we observed that the loss of *TP53* resulted in a reduction in erythroid colony formation and an enhanced replating potential of CFU-GMs compared with shSCR (Figure 2B). In this context, the effect of *TP53* reduction was also linked to the immature stem cell−enriched $CD34^+/CD38^-$ fraction (Figure 2C), which is in line with the significantly higher stem cell frequency on *TP53* removal (Figure 2D).

Taken together, these findings indicate that loss of function or presence of $TP53^{R273H}$ provides improved preservation of the in vitro stem cell potential that is restricted to the immature $CD34^+/CD38^-$ cell fraction, which is in line with murine data [18].

When comparing $TP53^{R273H}$ and sh*TP53*, we find that the effects on CB $CD34^+/CD38^-$ colony formation are comparable, although *TP53* mutations have been associated with oncogenic gain-of-function, which is concluded mostly from studies in solid tumors [3]. To study the induced alterations in HSPCs we performed RNA sequencing from CB $CD34^+/CD38^-$ cells to compare the transcriptional programs induced by $p53^{R273H}$ and sh*TP53* (Figure 3A). Forty-eight to 72 hours after transduction of CB $CD34^+$ cells, we sorted GFP^+ $CD34^+/CD38^-$ directly in RNA lysis buffer. Expression of either $p53^{R273H}$ or sh*TP53* did not visually alter $CD34^+/CD38^-$ percentages between samples (FACS data not shown, Gerritsen, 2019). Compared with control transduced cells, we found aberrant expression of 25 genes in sh*TP53* cells including classic p53 targets *CDKN1A* and *PHLDA3*. Of these 25 differentially expressed genes, 24 were downregulated. Also, when functionally annotating these 24 downregulated genes, the most significantly affected pathway caused by loss of *TP53* (sh*TP53*) was the p53 downstream pathway (Supplementary Figure E2A**,** online only, available at www.exphem.org) and, in particular, decreased expression of pro-apoptotic genes. In contrast, expression of $TP53^{R273H}$ was associated with decreased expression of genes involved in ribosome biogenesis and metabolism ($n = 20$) (Supplementary Figure E2B, online only), but with increased expression of genes involved in plasma membrane binding, extracellular structure organization, and differentiation ($n = 209$) (Supplementary Figure E2C, online only). Specifically, genes involved in differentiation include genes involved in megakaryocyte differentiation but also negative

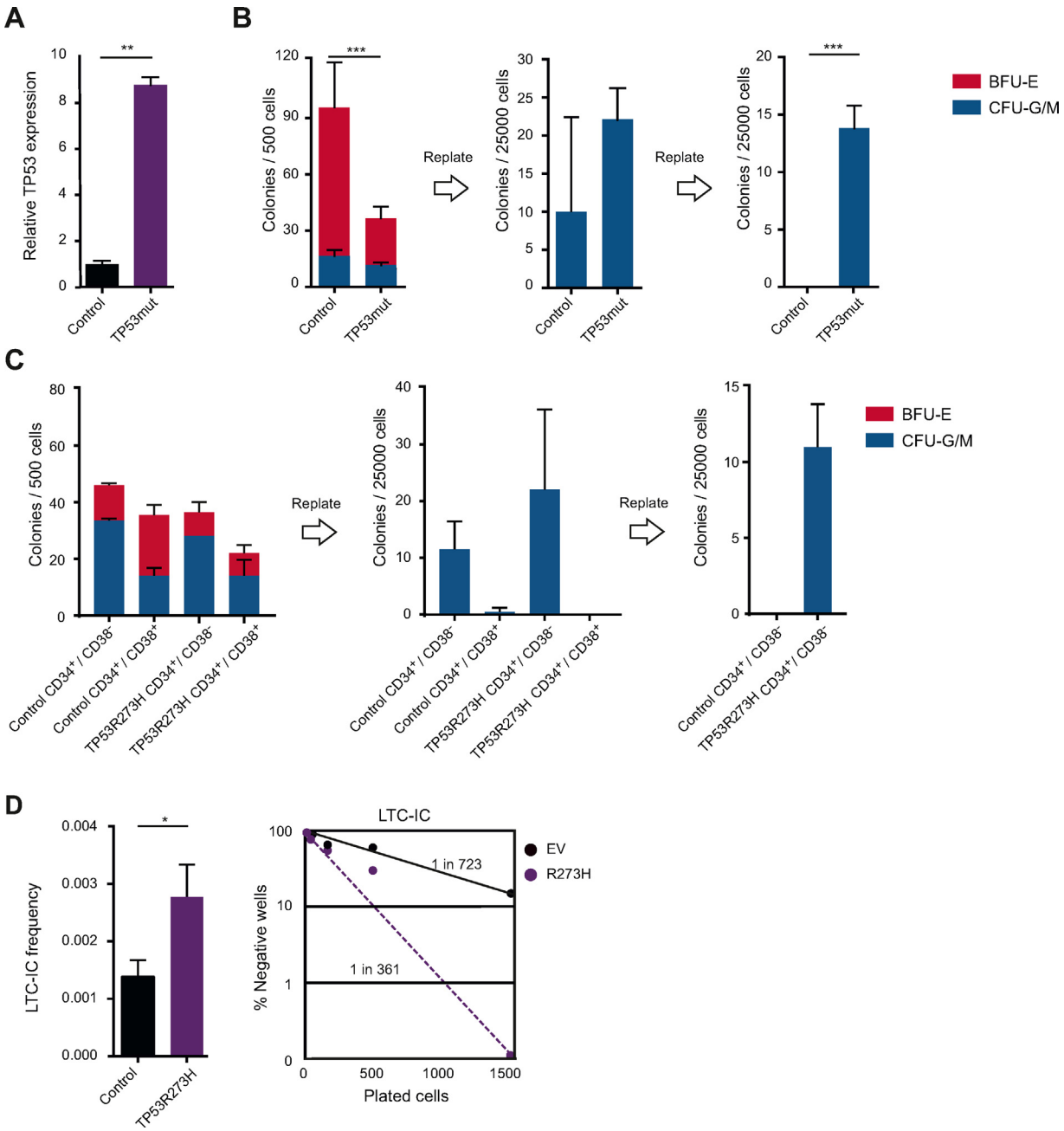

Figure 1 TP53mut cells have increased replating potential and stem cell frequency. **(A)** Expression of *TP53* was determined by reverse transcription quantitative polymerase chain reaction after $TP53^{R273H}$ overexpression ($n = 2$). **(B)** Colony formation and replating potential of CB transduced with control vector or $TP53^{R273H}$ overexpression vector. *Red*: Burst-forming units erythroid (BFU-E). *Blue*: Colony-forming units granulocyte/macrophage (CFU-G/M) ($n = 3$). **(C)** Colony formation and replating potential of CB transduced with control vector or $TP53^{R273H}$ overexpression vector sorted for more immature ($CD34^+/CD38^-$) or more mature populations ($CD34^+/CD38^+$) ($n = 3$). **(D)** Long-term culture-initiating colony assay (LTC-IC) reveals increased stem cell frequency in CB transduced with $TP53^{R273H}$ ($n = 3$). *CB*=cord blood.

regulators of myeloid differentiation. Interestingly, these represented mostly genes not annotated as p53 target before. Overlapping these two groups revealed only an overlap of four genes, suggesting the activation of different gene programs in response to *TP53* deletion as compared with the presence of $TP53^{mut}$ (Figure 3B).

Differential gene expression of genes on $TP53^{R273H}$ expression may suggest alternative p53 mutant binding, which can be assessed by chromatin immunoprecipitation sequencing. In view of the cell numbers required for this assay, we determined p53 binding in three cell lines: MOLM13 ($TP53^{wt}$), NB4 ($TP53^{R248Q}$), and Mono-Mac-6

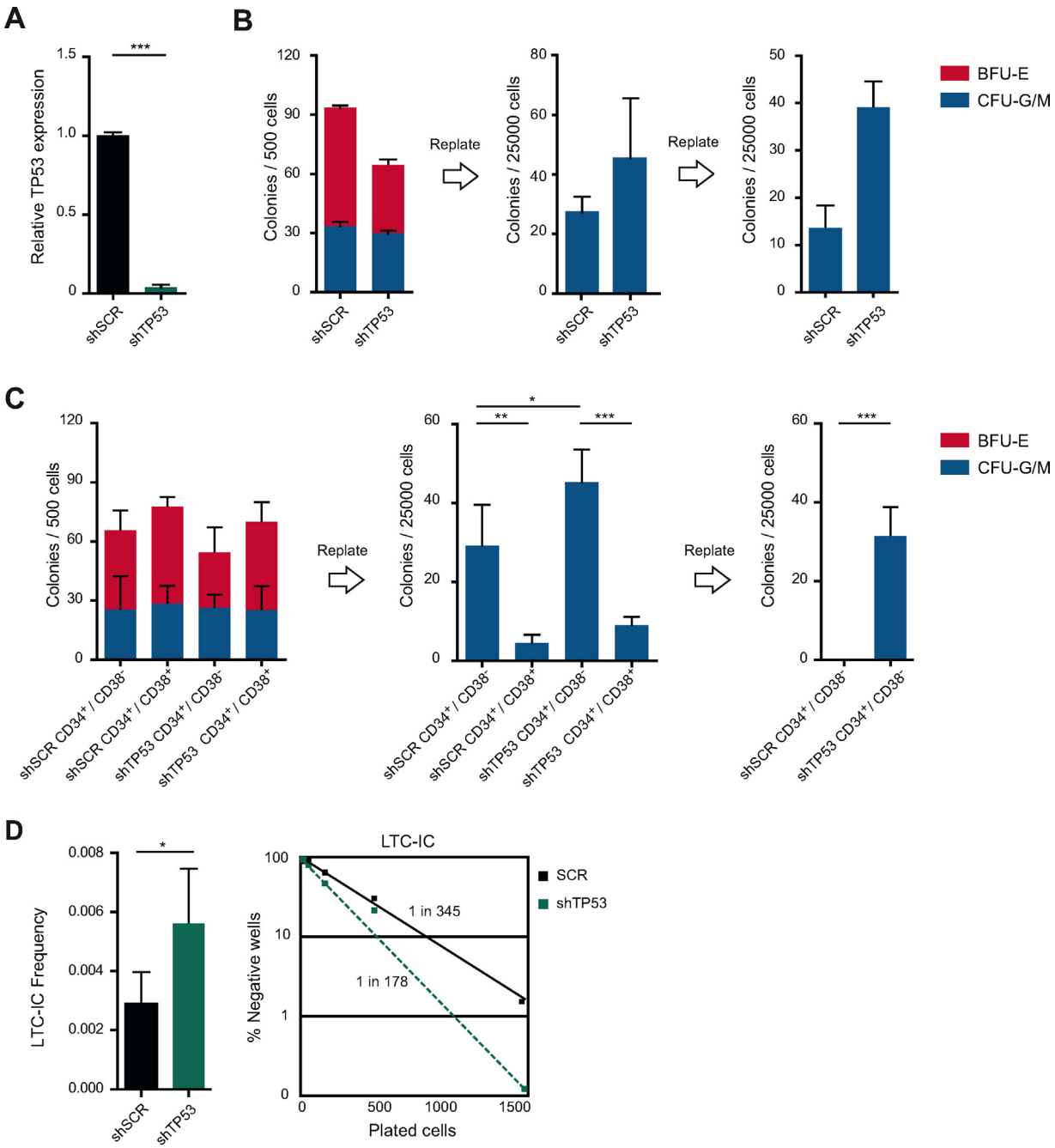

Figure 2 Downmodulation of TP53 increases stem cell maintenance similarly to TP53^{mut}. **(A)** Expression of *TP53* was determined by reverse transcription quantitative polymerase chain reaction after sh*TP53* (n = 2). **(B)** Colony formation and replating potential of CB transduced with shSCR or sh*TP53. Red* = burst-forming units–erythroid (BFU-E). *Blue* = colony-forming units granulocyte/macrophage (CFU-G/M) (n = 3). **(C)** Colony formation and replating potential of CB transduced with shSCR or shTP53 sorted for more immature (CD34$^+$/CD38$^-$) or mature (CD34$^+$/CD38$^+$) populations (n = 3). **(D)** Long-term culture-initiating colony assay (LTC-IC) reveals increased stem cell frequency in CB transduced with shTP53 (n = 3).

(*TP53*^{R273H}). The mutations in NB4 and Mono-Mac6 are located in the DNA binding domain of TP53. In MOLM13 cells we identified 284 p53 binding sites representing classic p53 targets such as *CDKN1A* (Figure 3C, top). For the *TP53*^{mut} cell lines NB4 and Mono-Mac-6, we detected 33,729 and 888 binding sites, respectively, which consists mostly of previously unreported sites (Figure 3C, bottom). P53 binding sites, in both *TP53*^{wt} and *TP53*^{mut} cell lines, were very strongly associated with H3K4me3 and H3K27ac, but not with H3K27me3 (Supplementary Figure E2D, online only), suggesting binding at open and accessible chromatin

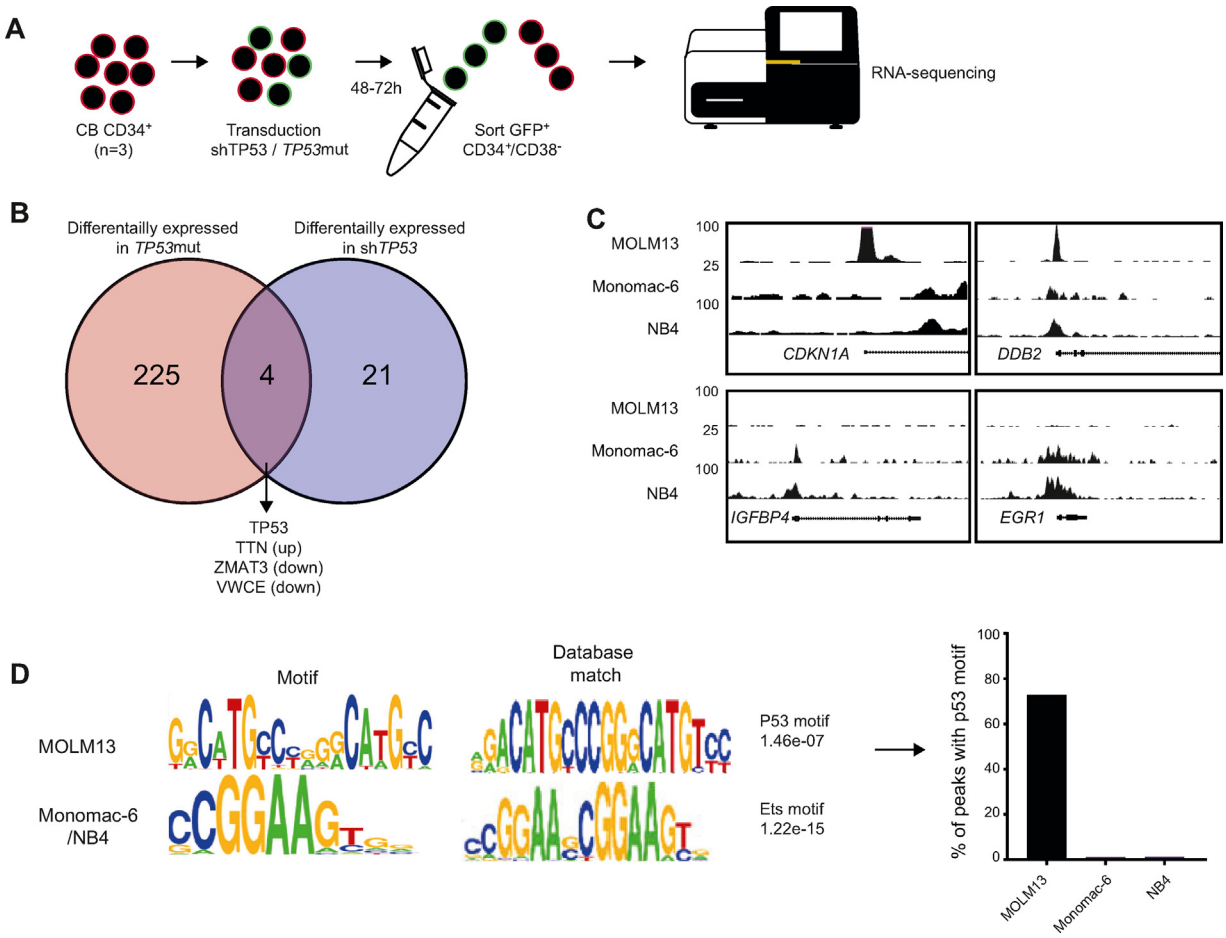

Figure 3 RNA sequencing of TP53^{R273H} and sh*TP53* and p53 binding motif analysis. **(A)** Experimental setup of RNA-sequencing experiments. **(B)** Overlap of differentially expressed genes in *TP53*^{mut} and sh*TP53*. **(C)** Screenshots of different genomic locations where there is binding of TP53^{wt} or TP53^{mut}. **(D)** Left: Motif analysis by GimmeMotif in MOLM13 (wt) and NB4/Monomac-6 (mut). Right: Percentage of peaks that contain a p53 binding motif.

regions. Because of the heterogeneity between the different cell lines, we explored the binding specificity of p53 within each of the cell lines. Motif search using GimmeMotifs [19] verified the presence of the full p53 motif (2 × 10-bp motif, 5′-PuPuPuC(A/T)(T/A)GPy-PyPy-3′, separated by 0–13 bp) [20] in 73% of MOLM13 binding sites, while in NB4 and Mono-Mac-6, the ETS binding motif was enriched and the p53 binding site motif was present in less than 1% of the peaks (Figure 3D). This suggests that mutant p53 is likely to bind a vast amount of DNA that does not have a p53 binding motif, unlike wild-type (WT) p53.

Next, we verified whether the observed findings of mutant p53 in HSPC and cell lines were also present in patient AML cells (which have also additional mutations) with and without *TP53* mutations. Therefore, we used three large available data sets (Blueprint [14] supplemented with five additional TP53 mutant AML [15], TCGA [16], and BeatAML [17]) and identified the differentially expressed genes between TP53^{mut} and TP53^{wt} AMLs for each database. Per data set, we detected differential gene expression between *TP53*^{mut} AMLs and *TP53*^{wt} AMLs. When overlapping the differentially expressed genes for all data sets, only 41 genes were identified that overlap between differentially expressed genes in all AML data sets studied (Figure 4A; Supplementary Table E2, online only, available at www.exphem.org). This suggests heterogeneity within *TP53*^{mut} AMLs, likely resulting from the heterogeneity in the genetic makeup of these cells and the differential effects of the type of *TP53* mutations (e.g., mutants in the DNA binding domain versus other domains). Further assessment of these genes revealed that they are linked to megakaryocyte differentiation and platelet formation (Figure 4B) and include GATA1, TAL1, and CD82. This is in line with findings that CD34^{+} cells of TP53^{mut} AMLs exhibit increased expression of genes involved in megakaryocyte and erythroid differentiation [21,22]. To further delineate the differential binding of p53, we studied primary AMLs with and without *TP53* mutation (n = 4) and performed ChIP sequencing against endogenous p53 (Supplementary Table E3, online only, available at www.exphem.org). We identified 1,356 peaks in *TP53*^{wt} and 1,171 peaks in *TP53*^{mut} primary AML samples, among which 356 overlap (Figure 4C). Unbiased motif discovery using GimmeMotifs [19] revealed enrichment for the p53 half-site motif (Figure 4D,E) in binding sites detected in *TP53*^{wt} AMLs, but not in binding sites detected in *TP53*^{mut} AMLs. This suggests altered binding properties of p53 due to the mutation. The genes that are associated with this decreased binding in TP53mut AMLs include

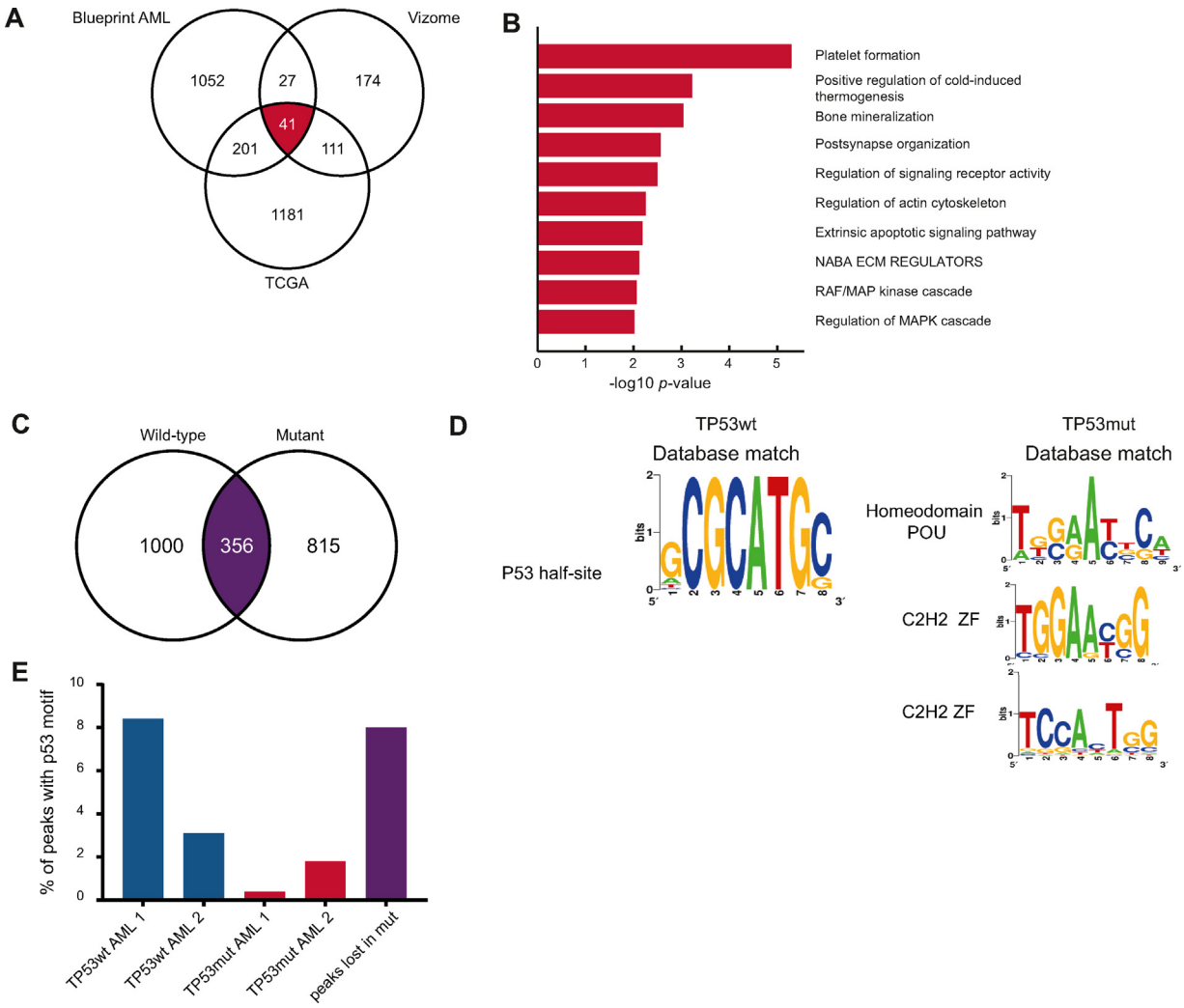

Figure 4 Chromatin immunoprecipitation (ChIP) sequencing and RNA sequencing data in primary acute myeloid leukemias (AMLs). **(A)** Overlap of differentially expressed genes in three databases (Supplementary Table E1, online only, available at www.exphem.org). **(B)** Go analysis of 41 commonly deregulated genes between three large cohorts. **(C)** Overlap of locations/genes that are bound by TP53^{mut} versus TP53^{wt} primary AML. **(D)** Motif analysis of TP53wt and TP53mut binding sites in primary AML. **(E)** Percentage of peaks in primary AMLs with a p53 motif.

some classic p53 targets such as *BAX and CDKN1A* (Supplementary Table E4, online only, available at www.exphem). All of these results indicate that in primary AML, p53 mutant has decreased binding to classic p53 targets, similar to the cell line models.

DISCUSSION

In our efforts to gain more insight into the mechanism of action of mutant p53, we functionally studied hematopoietic stem cells expressing*TP53*^{R27} [3], a frequently observed mutation, and loss of *TP53*. We observed that both loss of *TP53* expression and the presence of *TP53*^{R273H} lead to increased stem cell frequency and replating potential in the stem cell–enriched fraction. This might be linked to reduced p53-mediated apoptotic programming triggered by stress as a consequence of the in vitro applied assays. Although we focused on one specific mutation, our data are comparable to those from a recent study in which serial transplantation of *TP53*^{mut} HSPC in mice was performed [18]. This might give *TP53*^{mut} HSPCs a competitive advantage over normal HSPCs in the context of clonal hematopoiesis, but could also be important for the maintenance of leukemic stem cells. In addition to loss of function, the *TP53*^{R273H} triggered a number of additional programs in conjunction with an alteration of p53 binding sites in *TP53*^{mut} AMLs and *TP53*^{mut} cell lines. Here, the binding of p53 to the nonclassic binding sites may be linked to increased protein stability and altered protein complex formation. This could lead to a gain-of-function, as a large number of studies, mostly in solid tumors, have reported [1,3,4,6,23]. However, a recent study suggested that introduction of mutations into the *TP53* gene in *TP53*^{wt} cell lines leads to dominant negative loss-of-function, but not to gain-of-function [8]. Although we observed a loss of function, our data suggest that, at least in part, there may be a gain-of-function

effect of mutant p53, as we observed increased expression and additional binding of several genes not previously described as p53 mutant targets, in both CB ($p53^{R273H}$) and primary AMLs [24], including *TNS1* and *CD82* (Supplementary Table 2).

By using large AML expression data sets with a large mix of patients with concurrent molecular and genetic defects, a limited gene set was identified that was consistently expressed differentially in $TP53^{mut}$ AML. Remarkably, only a very small overlap was found between the different data sets. This suggests that the transcriptional effects conducted via the p53 pathway may be limited, Alternatively, the relatively low number of TP53 mutant AMLs in these data sets may be a limiting factor. Also, *TP53* mutant cells have more chromatin instability because of additional mutations, which will contribute to the final program observed in gene expression studies. Although some genes were linked to differentiation and cell signaling pathways, the most prominent association was the positive regulation of megakaryocytic development. We did not have the same observation in our cord blood cells. This might be due to how the heterogenous nature and different genetic backgrounds of AMLs might contribute to the observed differences. Also, previous studies had revealed an association between *TP53* mutations and erythroid development in leukemia. In acute erythroid leukemia, a high incidence of loss of WT *TP53* function is noted [21,25], and the presence of ring sideroblasts in secondary AML is frequently associated with *TP53* mutations [15].

In conclusion, in our models we were able to detect overlapping effects between $TP53^{mut}$ and loss of *TP53* on *in vitro* stem cell properties, but the effects on DNA binding and gene expression are distinct.

Conflict of Interest Disclosure

The authors declare that there is no conflict of interest regarding the publication of this article.

Acknowledgments

We are grateful to Dr. E. van den Berg, Department of Genetics, University Medical Centre Groningen, for providing the cytogenetic analysis and Dr. A. B. Mulder, Department of Laboratory Medicine, University Medical Center Groningen, for providing the mutation data analysis.

SUPPLEMENTARY MATERIALS

Supplementary material associated with this article can be found in the online version at https://doi.org/10.1016/j.exphem.2022.03.007.

REFERENCES

1. Brosh R, Rotter V. When mutants gain new powers: news from the mutant p53 field. Nat Rev Cancer 2009;9:701–13.
2. Leroy B, Anderson M, Soussi T. TP53 mutations in human cancer: Database reassessment and prospects for the next decade. Hum Mutat 2014;35:672–88.
3. Freed-Pastor WA, Prives C. Mutant p53: one name, many proteins. Genes Dev 2012;26:1268–86.
4. Walerych D, Lisek K, Sommaggio R, et al. Proteasome machinery is instrumental in a common gain-of-function program of the p53 missense mutants in cancer. Nat Cell Biol 2016;18:897.
5. Walerych D, Napoli M, Collavin L, Del Sal G. The rebel angel: mutant p53 as the driving oncogene in breast cancer. Carcinogenesis 2012;33:2007–17.
6. Zhu J, Sammons MA, Donahue G, et al. Prevalent p53 mutants co-opt chromatin pathways to drive cancer growth. Nature 2015;525:206–11.
7. Chen S, Wang Q, Yu H, et al. Mutant p53 drives clonal hematopoiesis through modulating epigenetic pathway. Nat Commun 2019;10:5649.
8. Boettcher S, Miller PG, Sharma R, et al. A dominant-negative effect drives selection of TP53 missense mutations in myeloid malignancies. Science 2019;365:599–604.
9. Prokocimer M, Molchadsky A, Rotter V. Dysfunctional diversity of p53 proteins in adult acute myeloid leukemia: Projections on diagnostic workup and therapy. Blood 2017;130:699–712.
10. Nangalia J, Mitchell E, Green AR. Clonal approaches to understanding the impact of mutations on hematologic disease development. Blood 2019;133:1436–45.
11. The Cancer Genome Atlas Network (TCGAR). Genomic and epigenomic landscapes of adult de novo acute myeloid leukemia. N Engl J Med 2013;368:2059–74.
12. Jasek M, Gondek LP, Bejanyan N, et al. TP53 mutations in myeloid malignancies are either homozygous or hemizygous due to copy number-neutral loss of heterozygosity or deletion of 17p. Leukemia 2010;24:216–9.
13. Liu Y, Chen C, Xu Z, et al. Deletions linked to TP53 loss drive cancer through p53-independent mechanisms. Nature 2016;531:471.
14. Yi G, Wierenga ATJ, Petraglia F, et al. Chromatin-based classification of genetically heterogeneous AMLs into two distinct subtypes with diverse stemness phenotypes. Cell Rep 2019;26:1059–69. e1056.
15. Berger G, Gerritsen M, Yi G, et al. Ring sideroblasts in AML are associated with adverse risk characteristics and have a distinct gene expression pattern. Blood Adv 2019;3:3111–22.
16. Papaemmanuil E, Gerstung M, Bullinger L, et al. Genomic classification and prognosis in acute myeloid leukemia. N Engl J Med 2016;374:2209–21.
17. Tyner JW, Tognon CE, Bottomly D, et al. Functional genomic landscape of acute myeloid leukaemia. Nature 2018;562:526–31.
18. Bondar T, Medzhitov R. p53-mediated hematopoietic stem and progenitor cell competition. Cell Stem Cell 2010;6:309–22.
19. van Heeringen SJ, Veenstra GJ. GimmeMotifs: a de novo motif prediction pipeline for ChIP-sequencing experiments. Bioinformatics 2011;27:270–1.
20. El-Deiry WS, Kern SE, Pietenpol JA, Kinzler KW, Vogelstein B. Definition of a consensus binding site for p53. Nat Genet 1992;1:45–9.
21. Montalban-Bravo G, Benton CB, Wang SA, et al. More than 1 TP53 abnormality is a dominant characteristic of pure erythroid leukemia. Blood 2017;129:2584–7.
22. Lu YC, Sanada C, Xavier-Ferrucio J, et al. The molecular signature of megakaryocyte–erythroid progenitors reveals a role for the cell cycle in fate specification. Cell Rep 2018;25:2083–93. e2084.
23. Olive KP, Tuveson DA, Ruhe ZC, et al. Mutant p53 gain of function in two mouse models of Li–Fraumeni syndrome. Cell 2004;119:847–60.
24. Fischer M, Steiner L, Engeland K. The transcription factor p53: Not a repressor, solely an activator. Cell Cycle 2014;13:3037–58.
25. Fagnan A, Bagger FO, Piqué-Borràs MR, et al. Human erythroleukemia genetics and transcriptomes identify master transcription factors as functional disease drivers. Blood 2020.